Measuring trapped noise in metamaterials

M. C. K. Wiltshire and R. R. A. Syms

Citation: Journal of Applied Physics **115**, 084905 (2014); doi: 10.1063/1.4866360
View online: http://dx.doi.org/10.1063/1.4866360
View Table of Contents: http://scitation.aip.org/content/aip/journal/jap/115/8?ver=pdfcov
Published by the AIP Publishing

Measuring trapped noise in metamaterials

M. C. K. Wiltshire[a] and R. R. A. Syms
Optical and Semiconductor Devices Group, Department of Electrical and Electronic Engineering, Imperial College London, Exhibition Road, London SW7 2AZ, United Kingdom

(Received 6 December 2013; accepted 8 February 2014; published online 26 February 2014)

Metamaterials constructed from conductive elements are lossy, and the structures act as sources of noise, whose spectrum is modified by the resonant nature of the medium itself. Furthermore, inside the medium, the noise is present as waves, which are standing waves for finite length samples. We present direct measurements of the noise spectra for a simple metamaterial comprising arrays of LC resonator elements, and compare them with the predictions of a circuit model incorporating Johnson noise. We find excellent agreement between the measured data and the model, reproducing both the resonant structure and the bandwidth of the noise spectrum, thus confirming the concept of noise waves in these metamaterials. These noise features match the frequency ranges where the metamaterial properties are useful, showing that noise is an inevitable companion to metamaterial performance in practical situations. © *2014 AIP Publishing LLC*.
[http://dx.doi.org/10.1063/1.4866360]

I. INTRODUCTION

Metamaterials[1–3] are artificial media that can be designed to provide electrical and magnetic properties outside the range normally encountered in nature. They consist of arrays of structures in which both the individual elements and the unit cell are small compared to the wavelength of operation; homogenization[4] of the structures then allows them to be described by the conventional electromagnetic constants of permittivity (ε) and permeability (μ), but with values that could not previously be obtained. For example, materials with simultaneously negative ε and μ can be built that have a negative refractive index,[5–7] and much attention has been given to the behaviour of such media[8] because they have the potential for sub-wavelength imaging.[9] Another concept enabled by metamaterials that has aroused substantial interest is cloaking,[10,11] in which any incident radiation is bent seamlessly around the cloaked object, thus rendering it totally invisible.

In order to generate a magnetic response, and in particular a negative magnetic response, metamaterials generally rely on a resonant current circulating in a conducting structure, for example the split-ring resonator (SRR)[3,12] which is widely used at microwave frequency. At lower frequency, the Swiss Roll structure[3,13] has been investigated, but has proved difficult to make in quantity. At higher frequency, the SRR becomes less effective, and the so-called fish-net structure[14] is commonly adopted. However, all these structures produce their magnetic response by virtue of resonant, circulating currents. Accordingly, it is useful to study the simplest implementation that can provide such an effect, the simple LC resonator circuit, the analogue of the SRR. This consists simply of a conducting loop or loops, completed by a suitable capacitor;[15,16] this may readily be patterned onto a printed circuit board (PCB).[17]

These structures do indeed generate a wide range of permeability values (ranging from $\mu = +30$ though zero to -30 in the case of the Swiss Rolls[18]), but they are inevitably lossy, because of the conducting elements within them. This loss manifests itself as signal attenuation, so that neither imaging nor cloaking can be perfect. In principle, it would be possible to compensate for the loss by including gain in the system,[19–21] but that is not a panacea, because, along with loss, there is always noise, and this is also amplified by the gain.

Noise is endemic in all electrical systems. It arises from thermal fluctuations of the current carriers and was first elucidated by Johnson[22] and Nyquist.[23] These authors showed that a resistor R at temperature T generates a noise voltage per unit bandwidth of

$$\langle V_n^2 \rangle = 4k_B TR, \tag{1}$$

where k_B is Boltzmann's constant. Some 25 years later, Callen and co-workers used statistical mechanics[24] and non-equilibrium thermodynamics[25] to generalise (1) into the Fluctuation-Dissipation Theorem (FDT).[26] This relates the fluctuations in a system at temperature T, with generalised coordinates X, acted on by generalised "force" F, to its generalised susceptibility χ, where $\chi = X/F$, through

$$\langle F^2 \rangle = 4k_B T\chi'', \tag{2}$$

where χ'' is the imaginary part of the susceptibility. Thus, the FDT links noise to loss. The fluctuations arise because when a "force" is applied at finite temperature, there is a continuum of states into which the system can move, whose probability of occupation is governed by Boltzmann statistics. Even when no "force" is applied, the system can lie in a range of states and can even move between these states when in thermal equilibrium. Thus, there are fluctuations in X and hence F which manifest themselves as noise.

How can we apply this to a practical system, for example, a sample of metamaterial? In principle, the FDT tells us

[a]Electronic mail: michael.wiltshire@imperial.ac.uk

how much noise will be generated, but it says nothing about the impact on the noise of the nature and size of the sample: this detail must all be contained in the susceptibility.[27] It is well-known that the shape of a sample alters its effective susceptibility (by the depolarising or demagnetising factors in the case of dielectric or magnetic objects), but what of the internal structure? After all, if the propagation of a signal is affected by the properties of the metamaterial, noise will be similarly affected. Furthermore, the noise generated inside the medium has to couple to the outside world to be observed, otherwise it will be trapped in the medium.

The core of this problem was tackled by Rytov,[28] who included noise sources (determined by the FDT) in the Maxwell curl equations. The solutions were expressed as Green's functions, which propagate through the medium as spherical waves, and are then integrated incoherently to obtain the resulting noise (see e.g., Ref. 29 for a standard text which also describes Rytov's theory). Although this formalism is rigorous, it is not easily used for treating practical problems. A more tractable theory has been developed by one of us and co-workers.[30,31] This was based on a finite, one dimensional model which permitted the integration in Rytov's theory to be replaced by a summation, thus rendering the problem exactly computable, and not limited to simple systems. Furthermore, in this approach, the noise is explicitly written in terms of the internal waves propagating in the system. For example, the magnetic response of the majority of metamaterials arises from resonant, current-bearing loops which have a finite resistance. Since the resistive element is in a resonant circuit, the noise spectrum will also be resonant.[32] If we have an array of such resistors, they will all generate a noise voltage and these must be added incoherently to obtain the total noise. Furthermore, if the elements are coupled, so that there is a spectrum of magneto-inductive[33] or electro-inductive[34] waves, the noise spectrum is also modified. Thus in metamaterial systems, where we rely on resonances and coupling to provide the exotic responses in the frequency range that we wish to exploit, the noise spectrum will be concentrated in just those same regions. The magneto-inductive waves couple to the electromagnetic waves that also propagate through the medium. The strength of this coupling determines how much of the magneto-inductive noise actually appears in the outside world; the rest is trapped in the medium.

Another model, based on an equivalent circuit approach, has been developed by Maslovski *et al.*[35] These authors reduce the entire medium to a single equivalent circuit, which allows them to calculate the external behaviour, in particular its radiative properties, but cannot reveal any internal details. Thus the trapped noise studied here cannot be addressed by this approach. Another equivalent circuit model has been developed[36] to study the effect of non-Foster elements in metamaterials, leading to predictions of the performance of active metamaterials, with gain incorporated in the system. Gain can be introduced to optical metamaterials by introducing a laser dye in the structure,[37] and the effect of noise on the lasing performance has been investigated,[38] although this is a highly non-equilibrium situation.

However, there have been no reports of experimental measurements of noise in metamaterials, so the aim of the present work is to investigate the noise spectrum of a simple metamaterial system, concentrating on the noise within the material, rather than that which is coupled to the outside world. We therefore investigate the magnetic noise arising from an array of resonant loops, as considered by Syms *et al.*,[30,31,39,40] by making direct measurements. In the conventional approach to noise measurement, a known, switchable, noise voltage is applied to the system, and the excess noise is derived from the combination of (sample-in, sample-out) and (noise source on, noise source off) states. This approach is suitable for characterising, for example, a metamaterial cable,[41] or even an imaging system,[42] but here we are concerned just with the noise generated within a passive material. Accordingly, rather than introducing a probe signal, we attempt a direct measurement of the noise. Because the unit cell of the metamaterial is quite large, we can place a suitable detector loop close to the sample, so that it is inductively coupled to the sample loops, and attempt to observe passively the excess noise picked up by this detector. Thus we need to include in our model not only the sample characteristics, but also those of the detector and the measurement system. In Sec. II, we describe our measurement approach in detail. In Sec. III, we describe the model and make a comparison with the measurements in Sec. IV. We discuss our results in Sec. V, and present our conclusions in Sec. VI.

II. MEASUREMENT

A. The samples and their parameters

Our samples consisted of arrays of four-turn coils, approximately 16×60 mm in size and spaced 20 mm apart, fabricated in double-sided PCB similar to those described in Ref. 17. The inductance, capacitance, and resistance of the single elements were derived by observing their resonant frequency and width of resonance (i.e., Q-factor) with different known values of added capacitance placed across the coils, and using small non-resonant loops for excitation and detection. From these data, we obtained an inductance $L = 1.36\,\mu$H and a self-capacitance of approximately 1.9 pF. The Q-factor of the unloaded coil is poor ($\sim$35) but increases with increasing values of capacitance placed across it, rising to $\sim$90 with a 47 pF surface-mount capacitor placed across the ends of the coil. This arrangement provides a series *LCR* resonator with a resonant frequency $f_0 = 19.4$ MHz. Strips of 20 such elements were fabricated, and from these we cut single elements, pairs of elements, triplets, and a strip of 19 elements (so that there we could measure both the centre and the end loops of the strip).

In addition to the properties of a single element, we need to determine the coupling between the elements. This is inductive, and falls off rapidly with separation. We made two sets of measurements to determine the coupling coefficients: first we used two separate single loops, whose resonant frequencies were measured as a function of their separation distance, and second we measured the resonant frequencies of the pairs and triplets described above. Both sets of experiments can be analysed to provide the nearest

neighbour and second neighbour coupling coefficients, κ_1 and κ_2 (where the mutual inductance between the elements is $M = \kappa L$). We find the nearest neighbour coupling to be $\kappa_1 = -0.109 \pm 0.003$ and the second neighbour coupling $\kappa_2 = -0.0085 \pm 0.0009$, an order of magnitude smaller. We also estimated the third neighbour coupling to be approximately $\kappa_3 \approx -0.002$, a factor of four smaller again, and so negligible within experimental error.

B. The measurement system and its parameters

The noise data were recorded using an Agilent N1996A spectrum analyser at 1001 points in the frequency range of 10–30 MHz, taking the rms value of 4096 scans. Since noise per unit bandwidth should be constant, we measured the spectra for five different bandwidths (1, 3, 10, 30, and 100 kHz), and then normalised the spectra to unit bandwidth. This was done for both background measurements (i.e., with no sample) and sample measurements; their difference was taken for each bandwidth and then their mean provided the final result.

The detector consisted of a probe loop, approximately 56×15 mm in size, constructed from RG-405 semi-rigid coaxial cable. The probe was held 4.2 mm above the PCB sample: this was a compromise between close coupling, which distorted the resonance of the sample element, and loose coupling which provided too little signal. Electrically, the detector consists of an *LCR* self-resonant loop of inductance L_d, capacitance C_d and resistance R_d, with the resonant frequency well above the region of interest, and a series capacitance C_s corresponding the connecting cable. We determined the values of these parameters by measuring the S_{11} spectrum using an Agilent 8753ES network analyser, calibrated with open, short and load attachments in place of the detector, and converting it to a measured impedance. This was fitted by an equivalent circuit to determine $L_\mathrm{d} = 19.7$ nH, $C_\mathrm{d} = 10.4$ pF, $R_\mathrm{d} = 0.88\,\Omega$, and $C_\mathrm{s} = 46.1$ pF for the loop inductance, capacitance and resistance, and series capacitance respectively.

We estimated the value of the detector—sample coupling parameters by measuring the transmission or S_{21} between two non-resonant loops placed $\sim$25 mm apart with the sample and detector between them. By recording spectra for the sample alone, the detector alone, and the detector coupled to the sample, and knowing the sample and detector parameters, it is possible to extract their coupling, which we found to be $\kappa_d = 0.395$. We note that the detector inductance is less than 1.5% of the sample inductance, so, despite its being quite closely coupled to the sample, we do not expect the presence of the detector to affect the sample properties significantly. Nevertheless, we noticed in these measurements that the resonant frequency of the sample actually increased in the presence of the detector by 0.22 MHz, whereas conventional coupled resonator theory requires that it should decrease (albeit very slightly). This was ascribed to the effect of the image current in the outer conductor of the detector when it is close by. We verified this by placing a strip of copper with an insulating backing film on top of the sample (without the detector loop present), and recording the resonant frequency: it increased by up to 0.34 MHz. As the copper strip was moved further away, the frequency reduced towards that of the bare sample. When the strip was placed 4.2 mm above the sample loop, the resonant frequency was again 0.2 MHz higher than that of the bare sample, showing that image current in the external conductor of the detector could indeed be acting to affect the resonant frequency of the sample loop. We account for this effect in our calculations by allowing the inductance of the sample loop to vary. However, the coupling between the sample and the detector should not be altered by the presence of any image currents, and so we write the sample inductance as $L + \Delta L$, where L is the self inductance found in the original characterisation and ΔL is a small variable self inductance, typically $<1\%$ of L, that mimics the effect of image currents in the detector and can also take into account any changes in self-capacitance or sample-to-sample variations.

The signal from the detector probe was amplified using two Spectrum Microwave QB-300 RF amplifiers (pre-amps) in series to provide a gain of 48 dB before being input to the spectrum analyser. The gain of the pre-amp pair was measured as a function of frequency using the network analyser to record an S_{21} spectrum, whereas the input impedance was determined from an S_{11} measurement.

Finally, the sample, detector, and first pre-amp had to be protected from any signals derived from the laboratory environment. Accordingly they were all placed inside a copper-lined box to shield the equipment from any external signals. It was found that copper walls had to be well-removed from the sample loops, otherwise they coupled to the walls and their resonance was quenched; we constructed a box from unprocessed PCB (single sided 1 oz copper (i.e., 35 μm thick) on FR4 board) with overall dimensions $90 \times 45 \times 30$ cm, so that all samples were at least 10 cm away from the walls. We ensured that all the joints between the walls were electrically connected by reinforcing them with copper tape with conducting adhesive, and the lid was connected to the walls through copper fingers to ensure electrical continuity throughout the enclosure.

C. Single element Spectrum

Using this equipment, we then measured the excess noise spectrum generated by a single element, with the result shown in Figure 1.

This clearly shows a resonance at 19.64 MHz but is distorted from a pure Lorentzian shape, becoming negative (i.e., the detector + sample generates less noise at the spectrum analyser than the detector alone) above the resonance. We therefore have to consider how much of this noise actually arises from the sample loop, and how much is due to the pre-amp and detector noise spectra being modified by the presence of a resonant loop sample. Accordingly, we now develop a simple model for the noise spectra and consider the size of the different contributions.

III. MODELLING

The modelling of this system is simple: we describe each component by the circuit parameters defined above, and with each resistive element there is associated a Johnson

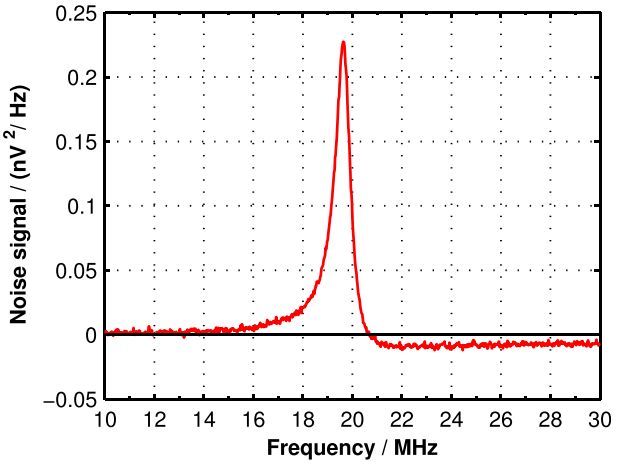

FIG. 1. Measured noise spectrum in nV^2/Hz as a function of frequency for a single element sample.

noise given by (1). We then apply Kirchhoff's circuit laws to calculate the current and hence the voltage that appears across the input of the preamplifier. The case for a single loop sample is shown in Figure 2. Here, the sample is shown as a loop containing L, C, R, and v_s; this is inductively coupled to the detector represented by a loop containing L_d, C_d, R_d, and v_d, with the series capacitance C_s in the pre-amp loop, in which the pre-amp itself is represented by its input impedance Z_p and an associated noise v_p. More complicated representations of the pre-amp and its noise are possible, and these are discussed later; for now we use the simpler model.

The circuit equations derived from applying Kirchhoff's laws are

$$\begin{pmatrix} Z_p' & -1/j\omega C_d & 0 \\ -1/j\omega C_d & Z_d & j\omega M_d \\ 0 & j\omega M_d & Z_s \end{pmatrix} \begin{pmatrix} I_0 \\ I_d \\ I_s \end{pmatrix} = \begin{pmatrix} v_p \\ v_d \\ v_s \end{pmatrix}, \quad (3)$$

where $Z_p' = Z_p + 1/j\omega C_d + 1/j\omega C_s$, $Z_d = j\omega L_d + R_d + 1/j\omega C_d$, $Z_s = j\omega L + R + 1/j\omega C$, and $M_d = \kappa_d\sqrt{L_d \cdot L}$ with $\kappa_d > 0$ for axial coupling. Then

$$\begin{pmatrix} I_0 \\ I_d \\ I_s \end{pmatrix} = \mathbf{Z}^{-1} \begin{pmatrix} v_p \\ v_d \\ v_s \end{pmatrix} = \mathbf{Y} \begin{pmatrix} v_p \\ v_d \\ v_s \end{pmatrix}, \quad (4)$$

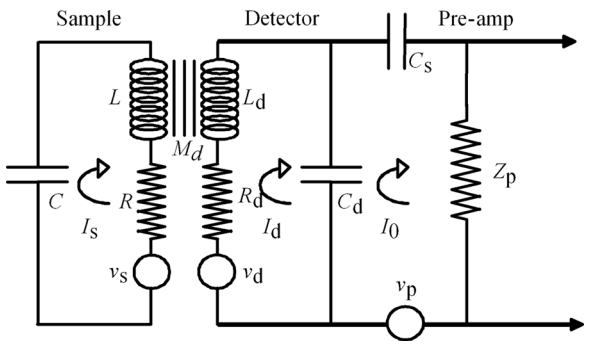

FIG. 2. The circuit for a resonant loop sample (L, C, R), coupled inductively via a mutual inductance M_d to the detector, that comprises an inductance, capacitance, and resistance (L_d, C_d, R_d) along with a series capacitance C_s. The detector provides an input to the preamplifier whose input impedance is Z_p. Each resistive element has a noise voltage v associated with it (see text).

where $\mathbf{Z}$ is the impedance matrix in (3) and $\mathbf{Y}$ is the admittance matrix. We calculate the contributions to the noise current in the input circuit, I_0, and hence to the noise voltage at the preamplifier input, from the sample loop v_s, the detector v_d and the preamplifier v_p and add these incoherently. Thus

$$v^2 = |Y_{1,1}v_pZ_p|^2 + |Y_{1,2}v_dZ_p|^2 + |Y_{1,3}v_sZ_p|^2. \quad (5)$$

We can now check that the observed noise in Fig. 1 is indeed due to the sample noise, the third term in (5), and not merely to the preamplifier noise being modified by the additional circuits (the first term in (5)). First, we obtain a set of the variable parameters that give a good representation of the total noise. Accordingly, we fixed the unperturbed sample inductance and capacitance, along with the detector parameters and pre-amp impedance, and allowed the perturbation of the sample inductance, ΔL, and the Q-factor to vary. To allow for the fact that noise from the pre-amp is determined in part by its active circuitry, whereas that of the detector and sample is purely Johnson noise, we also included a scaling parameter, β, on the pre-amp noise voltage in the calculation. The overall scale factor, α, was determined by minimising the residuals analytically, so that (5) becomes

$$v^2 = \alpha\left[\beta|Y_{1,1}v_pZ_p|^2 + |Y_{1,2}v_dZ_p|^2 + |Y_{1,3}v_sZ_p|^2\right]. \quad (6)$$

We then carried out a least-squares fit to determine the optimum values of these parameters, and, using them, investigated the relative sizes of the three contributions to (6). These are shown in Figure 3, from which it is clear that the sample noise does indeed dominate the measured spectrum around the resonance frequency.

We also note from Fig. 3 that, above the resonance frequency, the excess pre-amp noise is negative: adding the sample loop as shown in Fig. 2 reduces the noise measured by the pre-amp above the resonant frequency. This is because the Thévenin equivalent impedance of

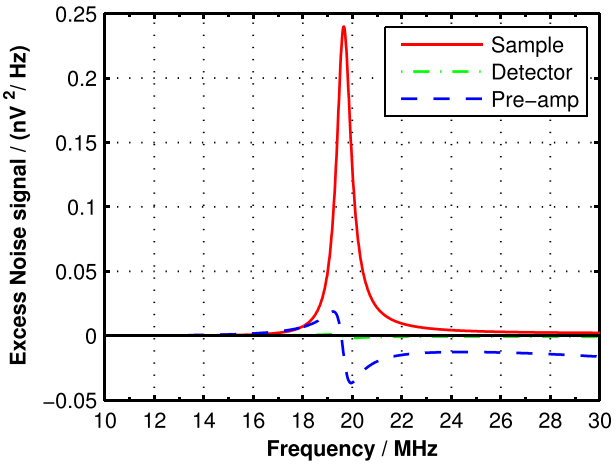

FIG. 3. Components of the excess noise spectrum in nV^2/Hz as a function of frequency for a single element sample. Red full line, sample noise; green chain line, excess detector noise; blue dashed line, excess pre-amp noise.

the detector is modified by the presence of the sample, being reduced below f_0 and increased above f_0. This impedance acts in combination with the pre-amp input impedance Z_p as a voltage divider on the pre-amp noise v_p, so when the Thévenin equivalent impedance is reduced, the voltage input to the pre-amp increases, and conversely when the Thévenin impedance is increased, the voltage input to the pre-amp is reduced, despite the pre-amp noise voltage remaining the same. This accounts for the apparently negative region of the observed noise spectrum in Fig. 1.

IV. COMPARISON WITH EXPERIMENT

Having established our model parameters and confirmed that the majority of the measured noise does arise from the sample, we can consider the noise from more complicated samples. In addition to the single elements, we have studied pairs, triplets, and a one dimensional array of 19 resonant elements that we also compare with the result of Syms *et al.*[39]

A. Single Element

As described above, we have measured the noise spectrum arising from a single element and matched it to the noise calculated using the circuit shown in Fig. 2 and Eqs. (3)–(6). The free parameters in the calculation were taken to be the perturbation of the sample inductance, ΔL, the Q-factor of the sample (which accounts for the perturbation of the sample resistance), and β, the scaling factor that describes the ratio of the pre-amp noise to the Johnson noise of the detector and sample. These parameters were determined by a least squares fit to the experimental data and are summarised in Table I. The resulting spectra are shown in Fig. 4(a), which shows an excellent match between theory and experiment.

B. Two Element Pair

When we study a pair of elements, we place the detector as before over one of the elements, and measure the resulting spectrum. This is shown in Fig. 4(b). In the model, we have to include the coupling between neighbouring elements, κ_1, as described in Sec. II A, and also the coupling, κ_{d2}, between the detector and the second neighbouring element (i.e., the one that does not have the detector placed above it). κ_{d2} could not be obtained reliably from the measurements described in Sec. II B so was left as a disposable parameter to be fitted. These two parameters affect the spectrum in quite different ways: κ_1 determines the splitting between the peaks, whereas κ_{d2} alters their relative intensity. In principle, it would be possible to fit κ_1 as well as κ_{d2}, but we have preferred to keep κ_1 fixed at the value determined in the measurements of Sec. II B, and only vary κ_{d2}. To do this, we extend (3) to include the second sample loop as follows:

$$\begin{pmatrix} Z_p' & -1/j\omega C_d & 0 & 0 \\ -1/j\omega C_d & Z_d & j\omega M_d & j\omega M_{d2} \\ 0 & j\omega M_d & Z_s & j\omega M_1 \\ 0 & j\omega M_{d2} & j\omega M_1 & Z_s \end{pmatrix} \begin{pmatrix} I_0 \\ I_d \\ I_{s1} \\ I_{s2} \end{pmatrix} = \begin{pmatrix} v_p \\ v_d \\ v_s \\ v_s \end{pmatrix}, \tag{7}$$

where $M_1 = \kappa_1 L$ and $M_{d2} = \kappa_{d2}\sqrt{L_d \cdot L}$ describe the nearest neighbour inter-element coupling and the detector–neighbouring inter-element coupling, respectively. We solve for the currents as before, and then add their contributions to the pre-amp input voltage incoherently as

$$v^2 = \alpha\left[\beta|Y_{1,1}v_pZ_p|^2 + |Y_{1,2}v_dZ_p|^2 + |Y_{1,3}v_sZ_p|^2 + |Y_{1,4}v_sZ_p|^2\right]. \tag{8}$$

The results are shown in Table I, and the spectra in Figure 4(b), which again shows an excellent match between theory and experiment.

C. Three elements

We can sample the noise spectrum arising from three elements in two ways: at the centre and at the end, and these generate different responses, which are shown in Figs. 4(c) and 4(d), respectively. When sampled at the centre, we only see two peaks due to symmetry (the even modes), but the end-sampled case shows all three peaks, as expected. In the model, we have to include the coupling between second nearest neighbours, κ_2, as described in Sec. II A. Broadly speaking, κ_1 determines the overall spread of the peaks, and κ_2 their asymmetry about the

TABLE I. Summary of parameters in the noise model.

Sample parameters: $L = 1.36\ \mu$H, $C = 49.2$ pF
Detector parameters: $L_d = 19.7$ nH, $C_d = 10.4$ pF, $R_d = 0.88\ \Omega$, and $C_s = 46.1$ Pf
Coupling parameters: $\kappa_1 = -0.109$, $\kappa_2 = -0.0085$, $\kappa_d = 0.395$
Fitting parameters:

Sample	Single	Pair	Triple-mid	Triple-end	19-mid	19-end
Q	27.9	47.6	44.5	51.7	60	67.7
$R\ (=\omega_0 L/Q)$	5.89	3.50	3.68	3.23	2.77	2.46
ΔL/nH	−29.0	2.55	−40.7	−0.67	−4.58	8.43
κ_{d2}		−0.043	−0.055	−0.078	−0.056	−0.026

central position. κ_d governs the overall strength of the coupling to the detector, whereas κ_{d2} determines the relative strengths of the peaks. Once again, we have only allowed κ_{d2} to vary. The model equations for the two cases become

$$\begin{pmatrix} Z_p' & -1/j\omega C_d & 0 & 0 & 0 \\ -1/j\omega C_d & Z_d & j\omega M_d & j\omega M_{d2} & 0 \\ 0 & j\omega M_d & Z_s & j\omega M_1 & j\omega M_2 \\ 0 & j\omega M_{d2} & j\omega M_1 & Z_s & j\omega M_1 \\ 0 & 0 & j\omega M_2 & j\omega M_1 & Z_s \end{pmatrix} \times \begin{pmatrix} I_0 \\ I_d \\ I_{s1} \\ I_{s2} \\ I_{s3} \end{pmatrix} = \begin{pmatrix} v_p \\ v_d \\ v_s \\ v_s \\ v_s \end{pmatrix}, \tag{9}$$

for the end-coupled case, and

$$\begin{pmatrix} Z_p' & -1/j\omega C_d & 0 & 0 & 0 \\ -1/j\omega C_d & Z_d & j\omega M_{d2} & j\omega M_d & j\omega M_{d2} \\ 0 & j\omega M_{d2} & Z_s & j\omega M_1 & j\omega M_2 \\ 0 & j\omega M_d & j\omega M_1 & Z_s & j\omega M_1 \\ 0 & j\omega M_{d2} & j\omega M_2 & j\omega M_1 & Z_s \end{pmatrix} \times \begin{pmatrix} I_0 \\ I_d \\ I_{s1} \\ I_{s2} \\ I_{s3} \end{pmatrix} = \begin{pmatrix} v_p \\ v_d \\ v_s \\ v_s \\ v_s \end{pmatrix}, \tag{10}$$

for the centre-coupled case. Here, $M_2 = \kappa_2 L$, and the remaining terms have the same meaning as before. As previously, we solve for the currents, and add their contributions incoherently as

$$v^2 = \alpha \left[\beta |Y_{1,1} v_p Z_p|^2 + |Y_{1,2} v_d Z_p|^2 + \sum_{n=1}^{3} |Y_{1,(2+n)} v_s Z_p|^2 \right]. \tag{11}$$

The results are shown in Table I, and the spectra in Figures 4(c) and 4(d). The match between theory and experiment is good, but the spacing of the peaks is not exactly correct, and hence the overall fit not as good as for the pair. We explored the possibility of allowing the inter-element coupling parameters to vary, but found that with the extra parameters the fit was ill-conditioned, with a long "valley" of minima for the sum of the squared residuals, so that the fitting routine could not reliably find an absolute minimum. Accordingly, we reverted to the original parameter set, and just varied ΔL, Q, κ_{d2}, and the relative voltage scale.

D. 19-element strip

Finally, we investigated the characteristics of a long strip of elements, such as would be used in magneto-inductive wave experiments. In this case, the noise that is localised on the individual elements in the previous cases, or propagates as waves in the infinite case, becomes standing waves in the finite length system. Again, we considered two cases: centre-coupled and end-coupled, and the spectra are shown in Figs. 4(e) and 4(f). The centre-coupled spectrum consists of nine peaks, again because of the symmetry of the arrangement in which only the even modes are seen (the odd modes can only be seen via κ_{d2}, the second neighbour coupling to the detector). In the end-coupled case, we should, in principle, be able to see all 19 possible modes, but are only able to resolve 14 of these. Moreover, the two spectra have quite different overall shapes: the centre-coupled spectrum has quite a uniform intensity distribution, whereas the intensity in the end coupled spectrum is concentrated at the low frequency end. Once again, we appeal to the model to reproduce these spectra. The equations now become

$$\begin{pmatrix} Z_p' & -1/j\omega C_d & 0 & 0 & 0 & 0 & \cdots & 0 \\ -1/j\omega C_d & Z_d & j\omega M_d & j\omega M_{d2} & 0 & \cdots & \cdots & 0 \\ 0 & j\omega M_d & Z_s & j\omega M_1 & j\omega M_2 & 0 & \cdots & 0 \\ 0 & j\omega M_{d2} & j\omega M_1 & Z_s & j\omega M_1 & j\omega M_2 & \cdots & 0 \\ 0 & 0 & j\omega M_2 & j\omega M_1 & Z_s & j\omega M_1 & \cdots & 0 \\ 0 & \vdots & 0 & j\omega M_2 & j\omega M_1 & Z_s & \cdots & 0 \\ \vdots & \vdots & \vdots & \vdots & \vdots & \vdots & \ddots & \vdots \\ 0 & 0 & 0 & 0 & 0 & 0 & \cdots & Z_s \end{pmatrix} \begin{pmatrix} I_0 \\ I_d \\ I_1 \\ I_2 \\ I_3 \\ I_4 \\ \vdots \\ I_N \end{pmatrix} = \begin{pmatrix} V_0 \\ v_d \\ v_s \\ v_s \\ v_s \\ v_s \\ \vdots \\ v_s \end{pmatrix}, \tag{12}$$

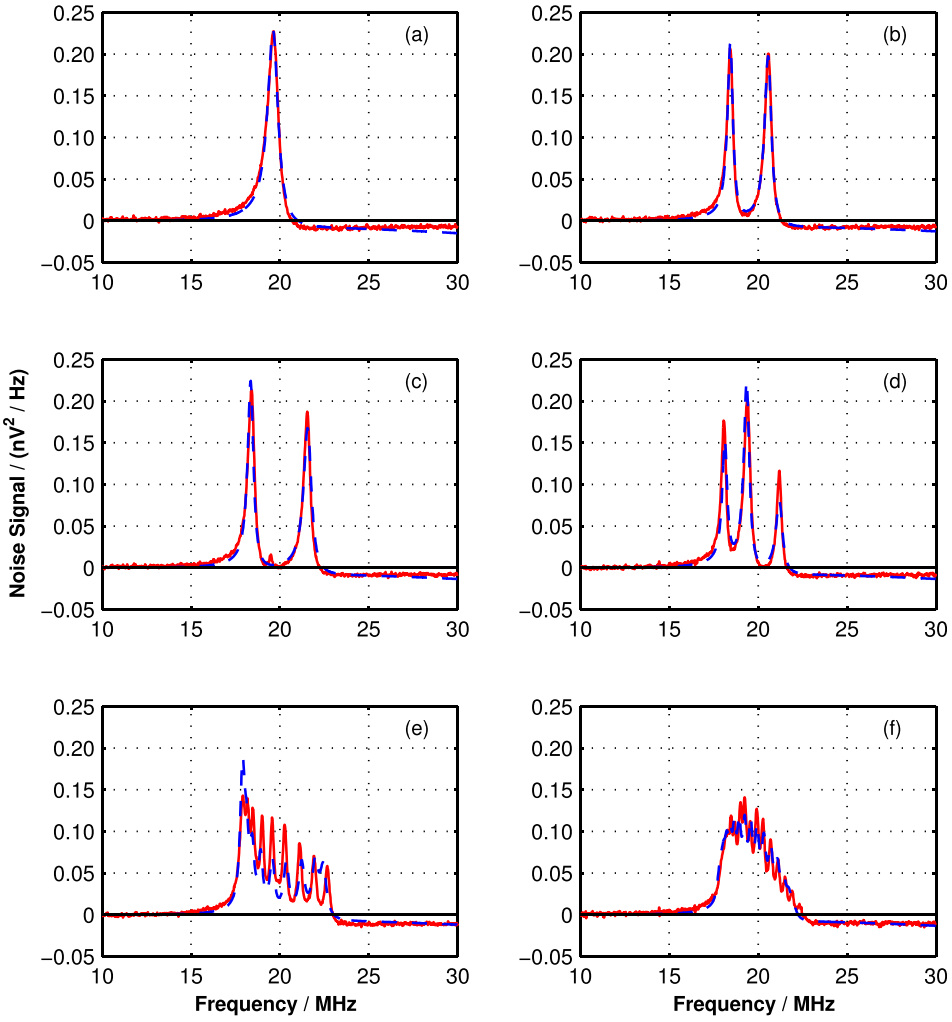

FIG. 4. Comparison of measured and calculated excess noise spectra in nV^2/Hz as a function of frequency for (a) a single element, (b) a pair of elements, (c) a triplet of elements, sampled at the centre, (d) a triplet of elements, sampled at the end, (e) a line of 19 elements, sampled at the centre, (f) a line of 19 elements, sampled at the end. Full red line, measured noise spectra; dashed blue line, calculated noise spectra.

for the end-coupled case and

$$\begin{pmatrix} Z_p' & -1/j\omega C_d & 0 & 0 & 0 & \cdots & 0 & 0 & 0 & \cdots & 0 \\ -1/j\omega C_d & Z_d & 0 & 0 & 0 & \cdots & j\omega M_{d2} & j\omega M_d & j\omega M_{d2} & \cdots & 0 \\ 0 & 0 & Z_s & j\omega M_1 & j\omega M_2 & \cdots & \cdots & \cdots & \cdots & \cdots & 0 \\ 0 & 0 & j\omega M_1 & Z_s & j\omega M_1 & \ddots & \cdots & \cdots & \cdots & \cdots & 0 \\ 0 & 0 & j\omega M_2 & j\omega M_1 & Z_s & \ddots & \ddots & \cdots & \cdots & \cdots & 0 \\ \vdots & \vdots & \vdots & \ddots & \ddots & \ddots & \ddots & \ddots & \cdots & \cdots & \vdots \\ 0 & j\omega M_{d2} & \vdots & \vdots & \vdots & \ddots & Z_s & j\omega M_1 & j\omega M_2 & \cdots & 0 \\ 0 & j\omega M_d & \vdots & \vdots & \vdots & \ddots & j\omega M_1 & Z_s & j\omega M_1 & \ddots & 0 \\ 0 & j\omega M_{d2} & \vdots & \vdots & \vdots & \vdots & j\omega M_2 & j\omega M_1 & Z_s & \ddots & 0 \\ \vdots & \vdots & \vdots & \vdots & \vdots & \vdots & \vdots & \ddots & \ddots & \ddots & \vdots \\ 0 & 0 & 0 & 0 & 0 & \cdots & 0 & 0 & 0 & \cdots & Z_s \end{pmatrix} \begin{pmatrix} I_0 \\ I_d \\ I_1 \\ I_2 \\ I_3 \\ \vdots \\ I_9 \\ I_{10} \\ I_{11} \\ \vdots \\ I_{19} \end{pmatrix} = \begin{pmatrix} V_0 \\ v_d \\ v_s \\ v_s \\ v_s \\ \vdots \\ v_s \\ v_s \\ v_s \\ \vdots \\ v_s \end{pmatrix}, \tag{13}$$

for the centre-coupled case. As previously, we solve for the currents, and then add their contributions to the input voltage to the pre-amp incoherently as

$$v^2 = \alpha \left[\beta |Y_{1,1} v_p Z_p|^2 + |Y_{1,2} v_d Z_p|^2 + \sum_{n=1}^{19} |Y_{1,(2+n)} v_s Z_p|^2 \right]. \tag{14}$$

We were able to use the least squares fit to determine the parameters for the end-coupled case, reproducing the overall shape of the spectrum and the majority of the peaks within it. However, the fitting routine was unable to match the centrally coupled spectrum accurately enough, and tended to a single broad envelope. Accordingly, we fixed the Q value to ensure that the peaks were maintained and adjusted the other parameters to obtain a set of peaks that were at approximately the correct frequencies, although the underlying intensity of the spectrum was incorrect, and hence the quality of the fit was poor. The result of this matching is shown in Fig. 4(f).

V. DISCUSSION

The first point to emphasise in these results is that all the samples show a reduction in the noise signal (i.e., the excess noise is negative) above the resonance frequency (see Fig. 4). As a general principle, noise signals add incoherently, so negative contributions are impossible and would normally indicate a faulty measurement. However, as explained in Sec. III and Fig. 3, although the noise voltage from the pre-amp remains constant, the presence of the sample and the detector affects the noise measured: their Thévenin equivalent impedance acts as a voltage divider along with the pre-amp input impedance, thus allowing the signal at the pre-amp input to be reduced. This, of course, will be true for any signal, whether it be the noise signal we are considering here, or an information-bearing signal injected into the system: any signal reaching the pre-amp has been reduced by the voltage divider, so the reduction of noise seen here does not lead to an improvement in the signal-to-noise ratio.

The parameters in the noise model and from the fitting are summarised in Table I. We discussed the fixed parameters in Sec. II; here, we consider the ones derived from the fitting process. First, the Q-factor increases with the complexity of the sample, showing that the impact of the detector resistance on the overall sample resistance is reduced when more loops are added to the sample: the Q-factor of the sample loops in isolation is approximately 90. The parameter ΔL includes two components: the impact of image currents induced in the detector ground on the overall inductance of the sample and any change of self-capacitance arising from sample to sample variation (or indeed any change in the parasitic capacitances in the samples). The changes are small ($<1\%$ of the total self-inductance) but have a significant impact on the resonant frequency. For example, the value for the "Triple–mid" measurement appears to be an order of magnitude high in Table I, but reducing ΔL to -4 nH in this calculation shifts the spectrum down by 0.28 MHz. Accordingly, we just ascribe the spread of ΔL values to experimental variations. The coupling parameter κ_{d2} between the detector and its second neighbours affects the asymmetry of the peak intensities in the modelled spectra. Although it is small and typically only 10% of the main detector coupling parameter κ_d, with a value centred on $\kappa_{d2} = -0.05$, it depends sensitively on the precise placing of the detector with respect to the sample loops, and so we expect there to be some variation in this parameter.

The other two parameters relate to the relative magnitudes of the noise contributions and their overall scaling. We have adopted the simplest possible model for all the noise sources, just representing them as their Johnson noise arising from their resistance or the pre-amp input impedance, and then scaling these to match the experimental data. Thus, the sample and the detector noise voltages are scaled by a factor of $1/\beta$ or between 1.5 and 2 times over the pre-amp noise voltage, and the whole is scaled by about 20 to match the measurements. More sophisticated models exist: for example, Leach[43] describes the pre-amp noise as the combination of a voltage noise and a current noise (which are generally correlated). This model gives an accurate description of the background noise, based on direct measurements of the pre-amp noise with different input loads (short, open, or 50 Ω). However, in the present work, since we are only concerned with the excess noise generated when our detector probe is coupled to a sample element, and the simple model works extremely well, there is no need for a more complicated model.

It is only in the case of the 19-element sample, measured at its centre, that it has not been possible to fit the data accurately. Here, we observe 9 distinct modes, whose spacing and intensity depend on the precise coupling that exists both between elements and with the detector, and despite having constructed the largest feasible Faraday cage for the measurement, there remains the possibility of coupling to the walls of the enclosure, which would certainly modify the mode distribution pattern. As mentioned previously, a smaller enclosure quenched the signals, but here the effects may be more subtle, and certain modes more vulnerable to interaction with the enclosure than others. These measurements also show clearly that the noise exists as standing waves in the sample: by probing at the end of the sample, we measure all 19 possible modes, whereas measuring at the centre only allows the 9 symmetric modes to be observed.

Finally, we note that the results are consistent with the predictions of Syms and Solymar,[39,40] who calculate the noise for a single element and for a variety of arrays of elements, including a 15-element array, whose characteristics are very similar to those observed here in the 19-element array. It must be noted that Syms and Solymar[39,40] only consider the sample elements; here, we have included the effects of the detector and the preamp to obtain the measured noise spectrum.

VI. CONCLUSIONS

In conclusion, we have reported the direct measurement of noise in a simple metamaterial system, consisting of arrays of LC resonators. In these arrays, the noise exists as waves, which can be trapped in the system to form standing waves. Because of the size of the unit cell, these metamaterials allow the trapped noise to be measured using an inductive probe. The observed noise is a combination of the noise from the sample and the detector, along with that from the pre-amp. The latter is modified by the presence of the sample

and detector: the excess noise becomes negative above the resonant frequency because they act as a voltage divider on the pre-amp noise. A simple model, based on the Johnson noise of each component, has been used to explain the results. These show that the resonant elements generate a resonant noise spectrum, and when the elements are coupled, noise waves appear which become standing waves in finite length systems. These characteristics will have implications for the application of metamaterials, particularly when the signal is weak so that signal-to-noise performance is important.

ACKNOWLEDGMENTS

Support from the Leverhulme Trust through their award "Metamaterials and the Control of Electromagnetic Fields" was gratefully acknowledged.

[1]J. B. Pendry *et al*., "Extremely low frequency plasmons in metallic mesostructures," Phys. Rev. Lett. **76**(25), 4773–4776 (1996).
[2]J. B. Pendry *et al*., "Low frequency plasmons in thin-wire structures," J. Phys. Condens. Matter **10**(22), 4785–4809 (1998).
[3]J. B. Pendry *et al*., "Magnetism from conductors and enhanced nonlinear phenomena," IEEE Trans. Microwave Theor. Tech. **47**(11), 2075–2084 (1999).
[4]D. R. Smith and J. B. Pendry, "Homogenization of metamaterials by field averaging (invited paper)," J. Opt. Soc. Am. B **23**(3), 391–403 (2006).
[5]D. R. Smith *et al*., "Composite medium with simultaneously negative permeability and permittivity," Phys. Rev. Lett. **84**(18), 4184–4187 (2000).
[6]R. A. Shelby, D. R. Smith, and S. Schultz, "Experimental verification of a negative index of refraction," Science **292**(5514), 77–79 (2001).
[7]C. G. Parazzoli *et al*., "Experimental verification and simulation of negative index of refraction using Snell's law," Phys. Rev. Lett. **90**(10), 107401 (2003).
[8]D. R. Smith, J. B. Pendry, and M. C. K. Wiltshire, "Metamaterials and negative refractive index," Science **305**(5685), 788–792 (2004).
[9]J. B. Pendry, "Negative refraction makes a perfect lens," Phys. Rev. Lett. **85**(18), 3966–3969 (2000).
[10]J. B. Pendry, D. Schurig, and D. R. Smith, "Controlling electromagnetic fields," Science **312**(5781), 1780–1782 (2006).
[11]D. Schurig *et al*., "Metamaterial electromagnetic cloak at microwave frequencies," Science **314**(5801), 977–980 (2006).
[12]W. N. Hardy and L. A. Whitehead, "Split-Ring Resonator for use in Magnetic-Resonance from 200-2000 MHz," Rev. Sci. Instrum. **52**(2), 213–216 (1981).
[13]M. C. K. Wiltshire, "Radio frequency (RF) metamaterials," Phys. Status Solidi B **244**(4), 1227–1236 (2007).
[14]G. Dolling *et al*., "Low-loss negative-index metamaterial at telecommunication wavelengths," Opt. Lett. **31**(12), 1800–1802 (2006).
[15]M. C. K. Wiltshire *et al*., "Dispersion characteristics of magneto-inductive waves: comparison between theory and experiment," Electron. Lett. **39**(2), 215–217 (2003).
[16]M. C. K. Wiltshire *et al*., "Experimental and theoretical study of magneto-inductive waves supported by one-dimensional arrays of "swiss rolls"," J. Appl. Phys. **95**(8), 4488–4493 (2004).
[17]R. R. A. Syms, I. R. Young, and L. Solymar, "Low-loss magneto-inductive waveguides," J. Phys. D-Appl. Phys. **39**(18), 3945–3951 (2006).
[18]M. C. K. Wiltshire *et al*., "An effective medium description of 'Swiss Rolls', a magnetic metamaterial," J. Phys.-Condens. Matter **19**, 456216 (2007).
[19]R. R. A. Syms, L. Solymar, and I. R. Young, "Three-frequency parametric amplification in magneto-inductive ring resonators," Metamaterials **2**(2–3), 122–134 (2008).
[20]D. Langley, R. A. Coutu, Jr., and P. J. Collins, "Low-loss meta-atom for improved resonance response," AIP Adv. **2**(1), 012106 (2012).
[21]Y. Yuan, B.-I. Popa, and S. A. Cummer, "Zero loss magnetic metamaterials using powered active unit cells," Opt. Express **17**(18), 16135–16143 (2009).
[22]J. B. Johnson, "Thermal agitation of electricity in conductors," Phys. Rev. **32**(1), 97–109 (1928).
[23]H. Nyquist, "Thermal agitation of electric charge in conductors," Phys. Rev. **32**(1), 110–113 (1928).
[24]H. B. Callen and T. A. Welton, "Irreversibility and generalized noise," Phys. Rev. **83**(1), 34–40 (1951).
[25]H. B. Callen and R. F. Greene, "On a theorem of irreversible thermodynamics," Phys. Rev. **86**(5), 702–710 (1952).
[26]R. Kubo, "The fluctuation-dissipation theorem," Rep. Prog. Phys. **29**(1), 255 (1966).
[27]R. Kubo and K. Tomita, "A general theory of magnetic resonance absorption," J. Phys. Soc. Jpn. **9**, 888–919 (1954).
[28]S. M. Rytov, *Theory of Electric Fluctuations and Thermal Radiation* (Academy of Sciences, Moscow, 1953) [Translated as Air Force Cambridge Research Center TR-59-162].
[29]H. L. Pecseli, *Fluctuations in Physical Systems* (Cambridge University Press, 2000).
[30]R. R. A. Syms, O. Sydoruk, and L. Solymar, "Noise in one-dimensional metamaterials supporting magnetoinductive lattice waves," Phys. Rev. B **87**(15), 155155 (2013).
[31]R. R. A. Syms, O. Sydoruk, and L. Solymar, "Transmission-line model of noisy electromagnetic media," IEEE Trans. Microwave Theor. Tech. **61**(1), 14–22 (2013).
[32]J. R. Pierce, "Physical sources of noise," Proc. IRE **44**(5), 601–608 (1956).
[33]E. Shamonina *et al*., "Magnetoinductive waves in one, two, and three dimensions," J. Appl. Phys. **92**(10), 6252–6261 (2002).
[34]M. Beruete *et al*., "Electroinductive waves in chains of complementary metamaterial elements," Appl. Phys. Lett. **88**(8), 083503 (2006).
[35]S. I. Maslovski, C. R. Simovski, and S. A. Tretyakov, "Equivalent circuit model of radiative heat transfer," Phys. Rev. B **87**(15), 155124 (2013).
[36]Y. Fan, K. Z. Rajab, and Y. Hao, "Noise analysis of broadband active metamaterials with non-Foster loads," J. Appl. Phys. **113**(23), 233905 (2013).
[37]S. Xiao *et al*., "Loss-free and active optical negative-index metamaterials," Nature **466**(7307), 735–738 (2010).
[38]A. Pusch *et al*., "Coherent amplification and noise in gain-enhanced nanoplasmonic metamaterials: A Maxwell-Bloch Langevin approach," ACS Nano **6**(3), 2420–2431 (2012).
[39]R. R. A. Syms and L. Solymar, "Noise in metamaterials," J. Appl. Phys. **109**(12), 124909 (2011).
[40]R. R. A. Syms, O. Sydoruk, and L. Solymar, "Lossy metamaterials: No effective medium properties without noise," Phys. Rev. B **84**(23), 235150 (2011).
[41]R. R. A. Syms, K. Segkhoonthod, and I. R. Young, "Periodically structured thin-film cables," IETMicrowaves Antennas Propag. **5**(9), 1123–1129 (2011).
[42]M. J. Freire, R. Marques, and L. Jelinek, "Experimental demonstration of a mu = −1 metamaterial lens for magnetic resonance imaging," Appl. Phys. Lett. **93**(23), 231108 (2008).
[43]W. M. Leach, Jr., "Fundamentals of low-noise analog circuit design," Proc. IEEE **82**(10), 1515–1538 (1994).